Evolution of relativistic ions incessantly accelerated by an oblique shock wave

Shunsuke Usami and Yukiharu Ohsawa[a)]
Department of Physics, Nagoya University, Nagoya 464-8602, Japan

(Received 7 July 2003; accepted 20 November 2003)

The evolution of a large number of nonthermal, energetic particles that encounter with an oblique shock wave is studied with theory and simulations. First, an attempt is made to analytically discuss conditions under which particles can cross the shock front multiple times. Also, the change in the parallel momentum of a relativistic particle at the shock front is examined in detail. Then, the time variation of an energy distribution function of 5000 energetic particles is investigated with simulations; where field profiles are obtained from particle simulations of shock waves, and test particle orbits are calculated by use of these fields. The shock speed v_{sh} and propagation angle θ_0 are taken to be $v_{sh} \sim c \cos\theta_0$, for which incessant acceleration is expected. The development of these particles in the momentum space is also shown. © *2004 American Institute of Physics.*
[DOI: 10.1063/1.1641383]

I. INTRODUCTION

It has recently been shown with theory and numerical simulations that nonthermal, high-energy ions can be incessantly accelerated to much higher energies by an oblique shock wave.[1,2] In this mechanism, a relativistic effect plays an essential role; an effect that the particle velocity cannot exceed the speed of light c while the momentum can increase indefinitely. Because of this effect, the acceleration is especially enhanced[1–3] when the shock propagation speed, v_{sh}, is close to $c \cos\theta_0$

$$v_{sh} \simeq c \cos\theta_0 . \tag{1}$$

Here, the shock wave is supposed to propagate in the x direction in an external magnetic field $\boldsymbol{B}_0 = B_0(\cos\theta_0, 0, \sin\theta_0)$; the subscript 0 refers to the quantities in the upstream region. In such a shock wave, particles cannot quickly escape from the wave to the upstream region. Energetic particles can move with the shock wave for periods much longer than the gyroperiod and suffer the acceleration processes many times. This mechanism is different from the acceleration mechanisms of thermal hydrogen ions,[4–11] heavy ions,[12,13] and electrons.[14–16] In test particle simulations,[2] some ions were accelerated from $\gamma \sim 4$ to $\gamma \sim 160$, where γ is the Lorentz factor.

In a typical shock wave, the values of magnetic field B_z, transverse electric field E_y, and electric potential ϕ sharply rise in the shock transition region from those in the upstream region to those in the strong-field region. (This paper describes shock waves and particle acceleration processes in the laboratory frame, where the fluid velocities of electrons and ions are zero in the upstream region.) The width of the transition region, Δ, is of the order of the ion inertial length, c/ω_{pi}, for oblique shock waves,[17–22] where ω_{pi} is the ion plasma frequency. Energetic ions with speeds higher than v_{sh} have gyroradii much greater than Δ. After barely entering the shock wave, therefore, they can return to the upstream region. While they are in the strong-field region, their gyromotion is nearly parallel to the transverse electric field E_y. Hence, they gain energy there; the momentum perpendicular to the magnetic field, $p_\perp$, grows.[3,23] Provided that an energetic ion enters the strong-field region at $t = t_{in}$ and goes out to the upstream region at $t = t_{out}$, the increase in the Lorentz factor can be given as[1–3,23]

$$\delta\gamma = \frac{2 q_i p_{1\perp} E_{1y}}{m_i^2 c^2 \Omega_{i1}} \sin\left(\frac{\Omega_{i1}(t_{out} - t_{in})}{2\gamma} \right). \tag{2}$$

Here, q_i is the ion charge, and Ω_i is the nonrelativistic ion gyrofrequency; the subscript 1 refers to quantities in the strong-field region. After returning to the upstream region, these particles can go into the shock wave again because of the gyromotion. If the particle moves with the shock wave for a much longer time than its gyroperiod, this energy jump can occur many times; thus, the time variation of γ resembles a stairway.

On crossing the shock front, namely the thin transition region, the parallel momentum $p_\parallel$ goes up.[1,3,24,25] Because this is due to the magnetic structure, the particle energy does not change at this moment; $p_\perp$ decreases owing to the increase in $p_\parallel$ (if the initial $p_\parallel$ is positive). The particle can then get to move faster than the shock wave. That is, time-averaged particle velocity in the direction of the wave normal $\langle v_x \rangle$ exceeds v_{sh}, where $\langle v_x \rangle$ is given by $\langle v_x \rangle \simeq v_{0\parallel} \cos\theta_0$ with $v_{0\parallel}$ the velocity parallel to $\boldsymbol{B}_0$. This is the mechanism of escaping of accelerated particles from the shock wave. As mentioned earlier, however, particles cannot quickly escape from the shock wave to the upstream region when the condition (1) is satisfied.

The fast particle would spend most of the time in the upstream region in each gyroperiod, if it barely enters the shock wave. The acceleration time, $t_{out} - t_{in}$, would thus be much shorter than the gyroperiod, which is approximately

a)Electronic address: ohsawa@phys.nagoya-u.ac.jp

given by the gyroperiod $2\pi\gamma/\Omega_{i0}$. Then, it has been shown in a Letter[2] that the time rate of change of γ of a particle accelerated many times by a stationary shock wave is given as

$$\frac{d\gamma}{dt}=\frac{g_{01}}{\pi}\frac{v_{1\perp}v_{\rm sh}}{c^2}\Omega_{i0}, \tag{3}$$

where g_{01} is a numerical factor smaller than unity

$$g_{01}=\left(1-\frac{B_{z0}}{B_{z1}}\right)\left(1-\frac{B_{x0}^2}{2B_{z1}^2}\right)\sin\left(\frac{\Omega_{i1}(t_{\rm out}-t_{\rm in})}{2\gamma}\right). \tag{4}$$

Here, $d\gamma/dt$ was averaged over gyroperiod, $2\pi\gamma/\Omega_{i0}$, and it was assumed that $B_{z1}>B_{x0}$.

In the above work,[2] the motion and energy change of a particle that gained a great amount of energy was studied. In this paper, we consider a set of a large number of fast ions that are initially in the upstream region and investigate their development; i.e., what fraction of these particles can undergo the incessant acceleration and how their energies and momenta evolve with time. Also, we examine the motion of energetic particles in an oblique shock wave in more detail.

In Sec. II, we analytically discuss the conditions for particles to cross the shock front multiple times. We divide the velocity space into four regions, which are named A, B, C, and D. Particles that are initially in region A just move from the upstream to downstream region, crossing the shock front once; those in region B can cross the shock front multiple times; those in C or D are not overtaken by the shock wave if their initial positions are in the far upstream region. We show these regions in the velocity (or momentum) space and estimate the number of particles in region B. In addition, we study the change in the parallel momentum when a particle crosses the shock front. In Refs. 1 and 3, it was argued that $p_\parallel$ rises when the particle goes in and out of the shock region. In the simulation in Ref. 2, however, $p_\parallel$ went down when the particle entered the shock region. This discrepancy is resolved here. It is analytically shown that if the shock speed is sufficiently high, $p_\parallel$ can decrease at the moment when a fast particle goes in the shock wave. When the particle has returned to the upstream region, however, $p_\parallel$ becomes larger than the initial one; $p_{0\parallel}(t_{\rm out})>p_{0\parallel}(t_{\rm in})$. The magnitude of this increase is also estimated.

In Sec. III, we numerically study the evolution of energies and momenta of many fast particles. We use a model that is a hybrid between particle and test particle simulations.[2] That is, we obtain the electric and magnetic fields of a shock wave from one-dimensional, relativistic, electromagnetic particle simulations.[6,26] We then follow long-time trajectories of energetic particles in these fields. We observe how these particles evolve in the momentum space and how many particles can be accelerated to high energies. Of a set of 5000 energetic particles having the same initial energy $\gamma=4$ with an isotropic momentum distribution, 3.4% have been accelerated to energies $\gamma>50$ by $\Omega_{\rm H0}t=9000$, where $\Omega_{\rm H0}$ is the nonrelativistic hydrogen gyrofrequency, and the maximum energy has reached $\gamma\simeq 130$. In the momentum space, they basically evolve along the line given by $v_{0\parallel}\cos\theta_0=v_{\rm sh}$.

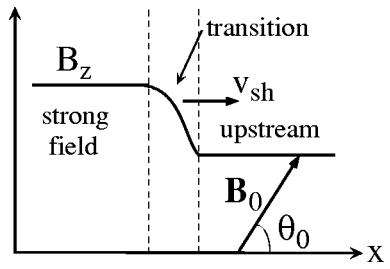

FIG. 1. Schematic shock profile. Shock waves are supposed to propagate in the x direction with speed $v_{\rm sh}$ in an external magnetic field $\boldsymbol{B}_0$ in the (x,z) plane.

Section IV gives a summary of our work. This acceleration process would become important in plasmas with rather strong magnetic fields (or low densities) such that the electron gyrofrequency is greater than the plasma frequency, $|\Omega_e|/\omega_{pe}>1$, as suggested by Eq. (1). Such plasmas could be found, for instance, in coronal magnetic tubes and around pulsars. The application to the latter would be particularly interesting because strong magnetosonic shock waves (or pulses) could be periodically generated there.

II. MOTION OF ENERGETIC IONS IN AN OBLIQUE SHOCK WAVE

We analytically study motions of fast ions whose speeds can be comparable to the speed of light c. We discuss the number of energetic particles crossing the shock front multiple times and the change in the parallel momentum. In the previous theory[3] on the parallel-momentum change, it was assumed that the shock propagation speed $v_{\rm sh}$ was much lower than the speeds of energetic particles. We here extend the theory so that $v_{\rm sh}$ can be of the order of speeds of fast particles.

A. Particles crossing a shock front

First, we examine conditions for particles to cross the shock front once or multiple times. As in Sec. I, we assume that a shock wave is propagating in the x direction ($\partial/\partial y=\partial/\partial z=0$) in an external magnetic field in the (x,z) plane, $\boldsymbol{B}_0=B_0(\cos\theta_0,0,\sin\theta_0)$ with $0°<\theta_0<90°$ (see Fig. 1). We then see that particles in the far upstream region will be caught up with by the shock wave if

$$v_{0\parallel}\cos\theta_0<v_{\rm sh}, \tag{5}$$

where $v_{0\parallel}=\boldsymbol{v}\cdot\boldsymbol{B}_0/B_0$; $v_{0\parallel}$ can be either positive or negative. Comparing the velocities in the x direction of particles and of the shock wave, we find that the particles with $v_{0\parallel}\cos\theta_0+v_{0\perp}\sin\theta_0<v_{\rm sh}$ cross the shock front only once, where $v_{0\perp}(>0)$ is the perpendicular particle speed. (Here, we neglect the effect of the change in $\boldsymbol{B}$ on particle motions. Also, we neglect the effect of $\boldsymbol{E}$.) That is, the particles with

$$v_{0\perp}<-\cot\theta_0(v_{0\parallel}-v_{\rm sh}/\cos\theta_0), \tag{6}$$

do not return to the upstream region once they penetrate the shock region. In Fig. 2, these particles are in region A; the left and right panels in Fig. 2 show velocity $(v_{0\parallel},v_{0\perp})$ and momentum $(p_{0\parallel},p_{0\perp})$ spaces, respectively.

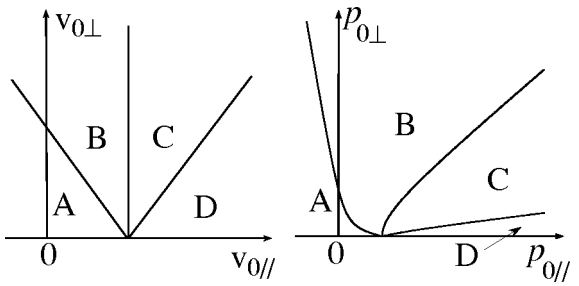

FIG. 2. Regions A–D in the velocity and momentum spaces. We consider particles that are initially in the upstream region. Particles in region A do not return to the upstream region, after entering the shock region. Particles in B may cross the shock front twice or more. Particles in C are not overtaken by the shock wave if their initial positions are in the far upstream region. Particles in D never encounter the shock wave.

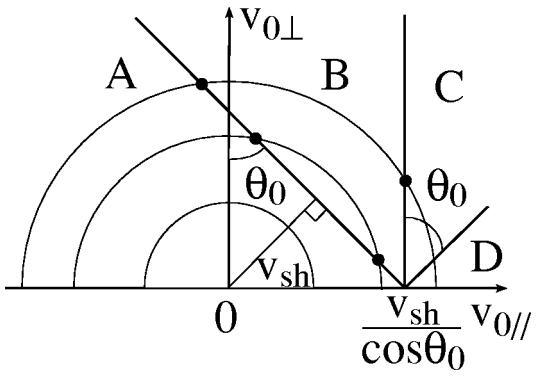

FIG. 3. Spherical surfaces and regions A–D on the $(v_{0\|},v_{0\perp})$ plane. The distance between the origin O and the boundary line of regions A and B is $v_{\rm sh}$. A spherical surface with $v>v_{\rm sh}/\cos\theta_0$ intersects with this line at a point with $v_{0\|}=v_{\|a}$ $(<v_{\rm sh}/\cos\theta_0)$ and intersects with the boundary line between regions B and C. A spherical surface with $v_{\rm sh}<v<v_{\rm sh}/\cos\theta_0$ has two intersection points with the line between A and B. If $v<v_{\rm sh}$, there is no intersection point.

Particles satisfying (5) and the relation $v_{0\perp}>-\cot\theta_0(v_{0\|}-v_{\rm sh}/\cos\theta_0)$ may cross the shock front twice or more, depending on the gyrophase at the moment of the encounter with the wave. These particles are in region B in Fig. 2. Some of them can undergo the incessant acceleration.

As for the case with $v_{0\|}\cos\theta_0>v_{\rm sh}$, particles with

$$v_{0\perp}<\cot\theta_0(v_{0\|}-v_{\rm sh}/\cos\theta_0) \tag{7}$$

will never encounter the shock wave even if their initial positions (in the upstream region) are very close to the shock front. These particles are in region D in Fig. 2. Region C represents particles that satisfy $v_{0\|}\cos\theta_0>v_{\rm sh}$ but do not meet (7). Particles in this region will not be overtaken by the shock wave if they are in the far upstream region initially. They may, however, enter the shock region because of the gyromotion if they are near the shock front.

In the momentum space $(p_{0\|},p_{0\perp})$, the relation $v_{0\|}\cos\theta_0=v_{\rm sh}$ can be written as

$$\frac{(c^2\cos^2\theta_0/v_{\rm sh}^2-1)p_{0\|}^2}{m_i^2c^2}-\frac{p_{0\perp}^2}{m_i^2c^2}=1, \tag{8}$$

with $p_{0\|}>0$. Also, the relations $v_{0\perp}=\pm\cot\theta_0(v_{0\|}-v_{\rm sh}/\cos\theta_0)$ can be expressed as

$$\frac{(p_{0\|}\cos\theta_0\mp p_{0\perp}\sin\theta_0)^2}{m_i^2\gamma_{\rm sh}^2v_{\rm sh}^2}-\frac{(p_{0\|}\sin\theta_0\pm p_{0\perp}\cos\theta_0)^2}{m_i^2c^2}=1, \tag{9}$$

where $\gamma_{\rm sh}=(1-v_{\rm sh}^2/c^2)^{-1/2}$. In the right panel of Fig. 2, the boundary between regions A and B is given by Eq. (9) with the lower signs with $p_{0\|}\cos\theta_0+p_{0\perp}\sin\theta_0>0$; because $p_{0\perp}>0$, this satisfies $v_{0\|}<v_{\rm sh}/\cos\theta_0$. The boundary between regions B and C is indicated by Eq. (8) with $p_{0\|}>0$. The boundary between regions C and D is shown by Eq. (9) with the upper signs with $p_{0\|}\cos\theta_0-p_{0\perp}\sin\theta_0>0$ $(v_{0\|}>v_{\rm sh}/\cos\theta_0)$.

We consider a spherical surface with a radius v and calculate the number of particles that are in region B on this surface. We introduce the angle α between the particle velocity and $\boldsymbol{B}_0$;

$$v\cos\alpha=v_{0\|}. \tag{10}$$

If $v>v_{\rm sh}/\cos\theta_0$, then, the boundary between regions A and B, $v_{0\perp}=-\cot\theta_0\,(v_{0\|}-v_{\rm sh}/\cos\theta_0)$, intersects with the spherical surface at $v_{\|a}$ given by

$$v_{\|a}=v_{\rm sh}\cos\theta_0-(v^2-v_{\rm sh}^2)^{1/2}\sin\theta_0\,. \tag{11}$$

The largest half circle in Fig. 3 corresponds to this case. The area of this surface in region B then may be calculated as

$$S=\int_{\alpha_b}^{\alpha_a}2\pi v^2\sin\alpha d\alpha=2\pi v^2(\cos\alpha_b-\cos\alpha_a), \tag{12}$$

where $\cos\alpha_b=v_{\rm sh}/(v\cos\theta_0)$ and $\cos\alpha_a=v_{\|a}/v$. The ratio of S to the total area $4\pi v^2$ of the spherical surface is, therefore,

$$\frac{S}{4\pi v^2}=\frac{\sin\theta_0}{2}\left[\frac{v_{\rm sh}\sin\theta_0}{v\cos\theta_0}+\left(1-\frac{v_{\rm sh}^2}{v^2}\right)^{1/2}\right]. \tag{13}$$

In the limit of $v/v_{\rm sh}\to\infty$, this ratio approaches $\sin\theta_0/2$.

If $v_{\rm sh}<v<v_{\rm sh}/\cos\theta_0$ (the middle half circle in Fig. 3), then, the boundary between regions A and B intersects with the spherical surface at

$$v_{\|b}=v_{\rm sh}\cos\theta_0+(v^2-v_{\rm sh}^2)^{1/2}\sin\theta_0\,, \tag{14}$$

as well as at $v_{\|a}$. We thus define α_b as $\cos\alpha_b=v_{\|b}/v$. Instead of Eq. (13), we now have

$$\frac{S}{4\pi v^2}=\left(1-\frac{v_{\rm sh}^2}{v^2}\right)^{1/2}\sin\theta_0\,. \tag{15}$$

For $v=v_{\rm sh}/\cos\theta_0$, either Eqs. (13) or (15) gives $S/(4\pi v^2)=\sin^2\theta_0$.

When $v<v_{\rm sh}$ (the smallest half circle in Fig. 3), the whole spherical surface is in region A. These particles cross the shock front only once.

Figure 4 shows the ratio $S/(4\pi v^2)$ as a function of $v/v_{\rm sh}$. The angle θ_0 was taken to be 60°. For $v/v_{\rm sh}<1$, no particles can cross the shock front twice or more. The quantity $S/(4\pi v^2)$ takes its maximum value, $\sin^2\theta_0$, at $v=v_{\rm sh}/\cos\theta_0$ and approaches the value $\sin\theta_0/2$ as $v/v_{\rm sh}\to\infty$.

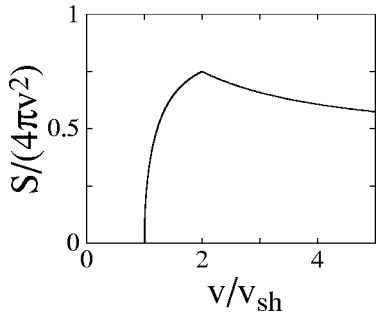

FIG. 4. Area S of spherical surface in region B as a function of the radius v.

B. Increase in parallel momentum

We consider a particle that enters the shock region at time $t=t_{\rm in}$ and, owing to the gyromotion, goes out again to the upstream region at time $t=t_{\rm out}$ (see Fig. 5). We then show that the parallel momentum of this particle always increases; $p_{0\parallel}(t_{\rm out})>p_{0\parallel}(t_{\rm in})$.

The gyroradius of the energetic ion is much larger than the width Δ of the shock transition region. The time rate of change of the magnetic field that the energetic ion feels along its orbit can therefore be expressed as

$$\frac{d\boldsymbol{B}}{dt}=(\boldsymbol{B}_1-\boldsymbol{B}_0)[\,\delta(t-t_{\rm in})-\delta(t-t_{\rm out})\,]. \tag{16}$$

Both $\boldsymbol{B}_0$ and $\boldsymbol{B}_1$ are assumed to be constant; $\boldsymbol{B}_1=B_1(\cos\theta_1,0,\sin\theta_1)$ with $B_1>B_0$ and $\theta_1>\theta_0$. In this section, we neglect the y component of $\boldsymbol{B}$, because it can have finite values only in the narrow transition layer.[14,18,19] In Fig. 6, we show $\boldsymbol{B}_0$, $\boldsymbol{B}_1$, and $\boldsymbol{v}$ at $t=t_{\rm in}$, projected on the (x,z) plane. Here, $\boldsymbol{e}_{x'}$ is the unit vector in the direction perpendicular to $\boldsymbol{B}_1$ and to the y axis; i.e., $\boldsymbol{e}_{x'}=\boldsymbol{e}_y\times\boldsymbol{B}_1/B_1$ where $\boldsymbol{e}_y$ is the unit vector in the y direction. Also, α_{xz} is the angle between $\boldsymbol{B}_0$ and the velocity projected on the (x,z) plane.

From the equation of motion, we have

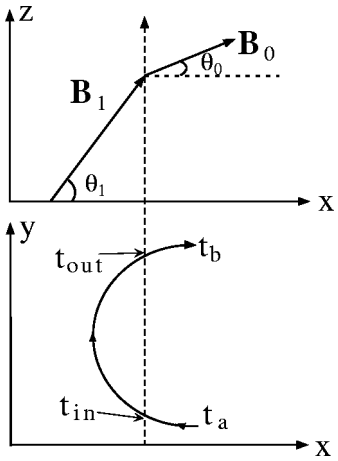

FIG. 5. Schematic diagram of magnetic fields and ion orbit. The upper panel shows the upstream magnetic field $\boldsymbol{B}_0$ and the field $\boldsymbol{B}_1$ in the strong-field region. The lower panel shows an ion orbit projected on the (x,y) plane, which goes in and out of the shock wave at $t=t_{\rm in}$ and $t=t_{\rm out}$, respectively.

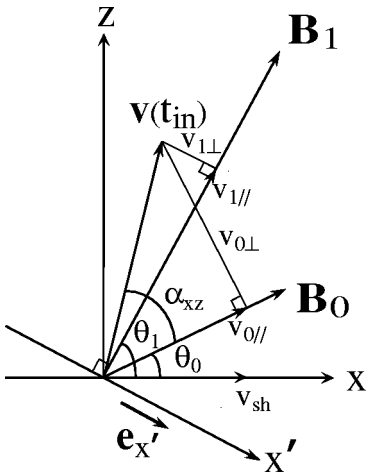

FIG. 6. Schematic diagram of magnetic fields and velocity at $t=t_{\rm in}$ projected on the (x,z) plane. Here, $v_{0\parallel}$ and $v_{1\parallel}$ are the components of $\boldsymbol{v}(t_{\rm in})$ parallel to $\boldsymbol{B}_0$ and $\boldsymbol{B}_1$, respectively. [$\boldsymbol{v}(t_{\rm in})$ can have the y component.] The unit vector $\boldsymbol{e}_x'$ is perpendicular to $\boldsymbol{B}_1$, and α_{xz} is the angle between $\boldsymbol{B}_0$ and $\boldsymbol{v}(t_{\rm in})$ projected on the (x,z) plane.

$$\frac{d(\boldsymbol{p}\cdot\boldsymbol{B})}{dt}=\boldsymbol{p}\cdot\frac{d\boldsymbol{B}}{dt}+q_i\boldsymbol{E}\cdot\boldsymbol{B}. \tag{17}$$

In the following, we will neglect the second term on the right-hand side of Eq. (17), because the parallel electric field is weak in magnetohydrodynamic waves. The effect of perpendicular electric field is, however, retained.

Substituting Eq. (16) into Eq. (17) and integrating over time from $t=t_a$ (the time right before $t=t_{\rm in}$) to $t=t_b$ (the time right after $t=t_{\rm out}$), we find that

$$[p_{0\parallel}(t_{\rm out})-p_{0\parallel}(t_{\rm in})]B_0=[\boldsymbol{p}(t_{\rm in})-\boldsymbol{p}(t_{\rm out})]\cdot(\boldsymbol{B}_1-\boldsymbol{B}_0). \tag{18}$$

Here, we have used the relations $p_{0\parallel}(t_b)-p_{0\parallel}(t_a)=p_{0\parallel}(t_{\rm out})-p_{0\parallel}(t_{\rm in})$ and $\boldsymbol{B}(t_a)=\boldsymbol{B}(t_b)=\boldsymbol{B}_0$.

When the energetic particle crosses the narrow transition layer of the shock wave, $\boldsymbol{p}_\parallel$ and $\boldsymbol{p}_\perp$ change stepwise owing to the change in the magnetic field from $\boldsymbol{B}_0$ to $\boldsymbol{B}_1$, even though $\boldsymbol{p}$ is continuous, $\boldsymbol{p}(t_{\rm in})=\boldsymbol{p}_0(t_{\rm in})=\boldsymbol{p}_1(t_{\rm in})$. Furthermore, because $q_i\boldsymbol{E}\cdot\boldsymbol{B}$ is neglected here, $p_{1\parallel}(t)$ is constant during the time from $t=t_{\rm in}$ to $t=t_{\rm out}$. We, therefore, have $\boldsymbol{p}(t_{\rm in})-\boldsymbol{p}(t_{\rm out})=\boldsymbol{p}_{1\perp}(t_{\rm in})-\boldsymbol{p}_{1\perp}(t_{\rm out})$. Then, noting that $\boldsymbol{p}_{1\perp}\cdot\boldsymbol{B}_1=0$, we have the change in the parallel momentum, $\delta p_\parallel=p_{0\parallel}(t_{\rm out})-p_{0\parallel}(t_{\rm in})$, as

$$\delta p_\parallel=[\boldsymbol{p}_{1\perp}(t_{\rm out})-\boldsymbol{p}_{1\perp}(t_{\rm in})]\cdot\boldsymbol{B}_0/B_0. \tag{19}$$

We introduce the quantity

$$p_{1\perp x'}=\boldsymbol{p}_{1\perp}\cdot\boldsymbol{e}_{x'}, \tag{20}$$

to put Eq. (19) into the form (see Fig. 6)

$$\delta p_\parallel=[p_{1\perp x'}(t_{\rm out})-p_{1\perp x'}(t_{\rm in})]\sin(\theta_1-\theta_0). \tag{21}$$

Using Eq. (21), we will show that $\delta p_\parallel$ is always positive. In Ref. 3, this was analytically discussed assuming that the shock speed $v_{\rm sh}$ was much smaller than the speeds of fast particles. In the following, however, $v_{\rm sh}$ can be comparable to particle speeds.

At the moment when the particle enters the shock region from the upstream region, the x component of the particle velocity must be smaller than the shock speed $v_{\rm sh}$;

$$v_{1\parallel}(t_{\rm in})\cos\theta_1 + v_{1\perp x'}(t_{\rm in})\sin\theta_1 < v_{\rm sh}, \tag{22}$$

where $v_{1\perp x'} = \boldsymbol{v}_{1\perp}\cdot\boldsymbol{e}_{x'}$. When the particle goes out to the upstream region, v_x must be greater than $v_{\rm sh}$;

$$v_{1\parallel}(t_{\rm out})\cos\theta_1 + v_{1\perp x'}(t_{\rm out})\sin\theta_1 > v_{\rm sh}. \tag{23}$$

In terms of momentum, (22) and (23) can be expressed as

$$p_{1\parallel}(t_{\rm in})\cos\theta_1 + p_{1\perp x'}(t_{\rm in})\sin\theta_1 < m_i\gamma(t_{\rm in})v_{\rm sh}, \tag{24}$$

$$p_{1\parallel}(t_{\rm out})\cos\theta_1 + p_{1\perp x'}(t_{\rm out})\sin\theta_1 > m_i\gamma(t_{\rm out})v_{\rm sh}. \tag{25}$$

Inequalities (24) and (25) clearly indicate that

$$p_{1\perp x'}(t_{\rm out}) > p_{1\perp x'}(t_{\rm in}), \tag{26}$$

because $p_{1\parallel}(t_{\rm in}) = p_{1\parallel}(t_{\rm out})$ and $\gamma(t_{\rm out}) > \gamma(t_{\rm in})$. [The electric field E_y would make $\gamma(t_{\rm out})$ greater than $\gamma(t_{\rm in})$.[2,23] Obviously, however, even when $\gamma(t_{\rm out}) = \gamma(t_{\rm in})$, the relation (26) holds.] Because $\theta_1 > \theta_0$, it follows from Eqs. (21) and (26) that $p_\parallel$ always increases,

$$\delta p_\parallel = p_{0\parallel}(t_{\rm out}) - p_{0\parallel}(t_{\rm in}) > 0. \tag{27}$$

We can obtain the relation among $\delta p_\parallel$, $\delta\gamma = \gamma(t_{\rm out}) - \gamma(t_{\rm in})$, and $\delta v_\parallel$. From the definition of the change in the parallel velocity, $\delta v_\parallel = m_i^{-1}[p_{0\parallel}(t_{\rm out})/\gamma(t_{\rm out}) - p_{0\parallel}(t_{\rm in})/\gamma(t_{\rm in})]$, we have the following relation:

$$\frac{\delta p_\parallel}{p_{0\parallel}(t_{\rm in})} = \frac{\delta v_\parallel}{v_{0\parallel}(t_{\rm in})} + \frac{\delta\gamma}{\gamma(t_{\rm in})}, \tag{28}$$

where we have assumed that $\delta p_\parallel / p_{0\parallel}(t_{\rm in})$ and $\delta\gamma/\gamma(t_{\rm in})$ are both small. Equation (28) suggests that $\delta p_\parallel$ can be positive if $\delta\gamma > 0$, even when $\delta v_\parallel \sim 0$. This can occur when, as a result of the acceleration, $v_{0\parallel}$ has become close to c, while γ increases because of the transverse electric field.

C. Sign of the change in parallel momentum

Simulations show that $p_\parallel$ increases at both $t = t_{\rm in}$ and $t = t_{\rm out}$ when $v_{\rm sh} < c\cos\theta_0$,[3] whereas it tends to decrease at $t = t_{\rm in}$ when $v_{\rm sh} \sim c\cos\theta_0$.[2] We here discuss this, considering a particle moving with an average velocity $\langle v_x\rangle$ close to the shock speed;

$$v_{0\parallel}\cos\theta_0 \simeq v_{\rm sh}. \tag{29}$$

Substituting Eq. (29) in the inequality $v_{0\parallel}^2 + v_{0\perp xz}^2 < c^2$, where $v_{0\perp xz}$ is the projection of $\boldsymbol{v}_{0\perp}$ on the (x,z) plane, we have $\tan^2\alpha_{xz} < c^2\cos^2\theta_0/v_{\rm sh}^2 - 1$, which leads to the relation

$$\cos\alpha_{xz} > v_{\rm sh}/(c\cos\theta_0). \tag{30}$$

The decrease in $p_\parallel$ at $t = t_{\rm in}$ means that $\boldsymbol{p}(t_{\rm in})\cdot\boldsymbol{B}_1/B_1 < \boldsymbol{p}(t_{\rm in})\cdot\boldsymbol{B}_0/B_0$. It is evident from Fig. 6 that this occurs when $\alpha_{xz} < (\theta_1 - \theta_0)/2$. This gives

$$\cos\alpha_{xz} > \cos[(\theta_1 - \theta_0)/2], \tag{31}$$

because $0° < \theta_0 < \theta_1 < 90°$.

If (30) and the relation

$$v_{\rm sh} > c\cos\theta_0\cos[(\theta_1 - \theta_0)/2] \tag{32}$$

both hold, then (31) is always met. That is, for shock waves with (32), parallel momenta of particles with (29) decrease at $t = t_{\rm in}$. [Nonetheless, relation (27) holds.]

If $v_{\rm sh}$ is small, we will have the relation $v_{0\perp} \gg v_{\rm sh} \sim v_{0\parallel}$ for energetic particles satisfying (29). Hence, α is close to 90°; thus, the possibility that α_{xz} satisfies (31) is quite low (this can occur when $|v_y| \gg v_{0\perp xz}$). In this case, $p_\parallel$ is likely to rise at $t = t_{\rm in}$, as discussed in Ref. 3.

D. Magnitude of $\delta p_\parallel$

We make a rough estimate of $\delta p_\parallel$ for a simple case where $\boldsymbol{p}_{1\perp}(t_{\rm in})$ is in the (x,z) plane and $\boldsymbol{p}_{1\perp}(t_{\rm in}) \simeq -\boldsymbol{p}_{1\perp}(t_{\rm out})$. This can occur when $v_{\rm sh} \simeq v_{1\parallel}\cos\theta_1$. [For some parameters, this condition will not be realized. For instance, the relation $v_{\rm sh} = v_{1\parallel}\cos\theta_1$ is not compatible with Eq. (1).] For a given $p_{1\perp}$, $\delta p_\parallel$ becomes the largest at this gyrophase and is given as $\delta p_\parallel = -2\boldsymbol{p}_{1\perp}(t_{\rm in})\cdot\boldsymbol{B}_0/B_0$. Since $p_y(t_{\rm in}) = 0$ for this case, we find $\delta p_\parallel$ from Fig. 6 as

$$\delta p_\parallel = 2p\,\sin[\alpha(t_{\rm in}) + \theta_0 - \theta_1]\sin(\theta_1 - \theta_0). \tag{33}$$

Here, we neglect the change in p. Thus, the parallel momentum at $t = t_{\rm out}$ is

$$p_{0\parallel}(t_{\rm out})/p = \cos[\alpha(t_{\rm in}) - 2(\theta_1 - \theta_0)]. \tag{34}$$

If this parallel momentum is large, then the particle would not return to the shock region, going away ahead of the shock wave. In particular, $p_{0\parallel}(t_{\rm out})/p$ becomes unity when $\alpha(t_{\rm in}) = 2(\theta_1 - \theta_0)$; for this case, the momentum $\boldsymbol{p}$ is parallel to $\boldsymbol{B}_0$ at $t = t_{\rm out}$.

III. NUMERICAL STUDIES

We now numerically study statistical properties of this acceleration mechanism. We follow orbits of many particles in electric and magnetic fields of a shock wave and observe how their positions, momenta, and energies vary with time. Since we want to see the long-time behavior of these particles, we use test particle simulations.[2] In this method, the electromagnetic fields in a shock wave are obtained from a one-dimensional, relativistic, electromagnetic, particle simulation with full ion and electron dynamics.[6,26] We then assume that the shock wave observed in the particle simulation steadily propagates with a constant speed $v_{\rm sh}$ (the value measured in the particle simulation) and calculate the orbits of many test particles in these fields for a much longer time than particle simulations can follow.

We do not use Rankine–Hugoniot conditions to obtain field profiles. A simple discontinuity model based on Rankine–Hugoniot conditions does not give information of B_y, E_x, or E_z. Also, it does not give spatial profiles of either B_z or E_y. Furthermore, we will not be able to assume normal Rankine–Hugoniot conditions because the fluid model itself is not valid in collisionless shock waves; around the shock region, the velocity distribution functions should be quite different from Maxwellians.

In doing the test particle simulations, we suppose that the number density of nonthermal energetic particles is much

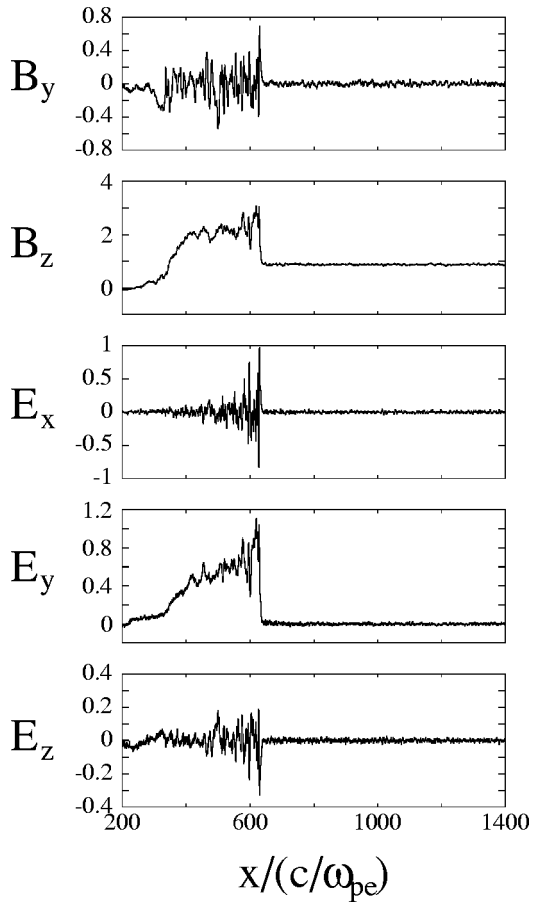

FIG. 7. Snapshots of field profiles in an oblique shock wave observed at $\omega_{pe}t=1000$ in the particle simulation. The field values are normalized to B_0. The shock propagation speed is $v_{\rm sh}=2.4v_{\rm A}$, and the propagation angle is $\theta_0=61°$.

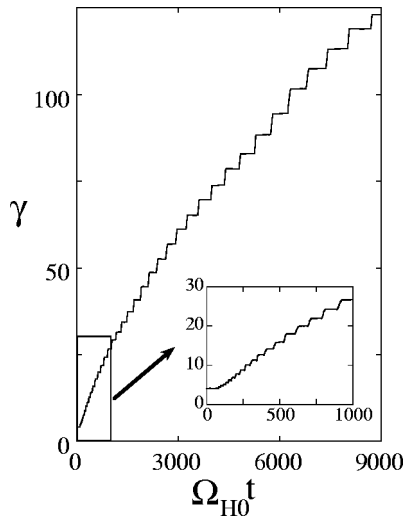

FIG. 8. Time variation of γ of an incessantly accelerated energetic ion. The small panel shows an expanded view of the early phase. The acceleration processes continued untill the end of the simulation.

lower than that of the background plasma; their effects on the wave evolution would therefore be negligible. We also note that synchrotron radiation power,

$$P\sim\frac{2q_i^2\Omega_{i0}^2v_{0\perp}^2}{3c^3}\gamma^2, \tag{35}$$

is much smaller than the energy gain rate given by Eq. (3). Their ratio is

$$\frac{P}{m_ic^2d\gamma/dt}\sim\frac{[v_{0\perp}^2/(cv_{1\perp})]\gamma^2}{6g_{01}Mn_i(c/\omega_{pi})^3}, \tag{36}$$

where M is the Alfvén Mach number, $M=v_{\rm sh}/v_{\rm A}$. For a plasma density $n_i=10^8$ cm^{-3}, the value of $n_i(c/\omega_{pi})^3$ is $\sim10^{18}$. Hence, the synchrotron radiation will be unimportant for particle energies $\gamma\lesssim10^9$.

The parameters of the particle simulation was as follows. The total system length was $L_x=8192\Delta_{\rm g}$, where $\Delta_{\rm g}$ is the grid spacing. The total number of electrons was $N_e=576\,000$; as in space plasmas, the code contained helium ions as well as hydrogen ions, and the helium number density was 10% of the hydrogen density. The ion-to-electron mass ratios were $m_{\rm H}/m_e=50$ and $m_{\rm He}/m_e=200$. (Because of the presence of helium ions, we were not able to choose a large hydrogen-to-electron mass ratio. The theoretical expression for the energy increase rate, (3), however, agrees with the simulation result with these mass ratios.[2]) The ratio of the electron gyrofrequency to the plasma frequency was $|\Omega_{e0}|/\omega_{pe}=1.5$ in the upstream region. The Alfvén speed is thus $v_{\rm A}/c=0.20$, where $v_{\rm A}$ is defined using the mass density in the H–He plasma. The electron skin depth was $c/(\omega_{pe}\Delta_{\rm g})=4$. The external magnetic field was in the (x,z) plane, $\boldsymbol{B}_0=B_0(\cos\theta_0,0,\sin\theta_0)$ with $\theta_0=61°$. The time step was $\omega_{pe}\Delta t=0.05$. We then excited a shock wave with $v_{\rm sh}=2.4v_{\rm A}$, which is close to $c\cos\theta_0$. The field profiles of this wave are shown in Fig. 7; $B_x=B_0\cos\theta_0$ is constant.

Using these fields propagating with the speed $v_{\rm sh}$, we followed the trajectories of test energetic hydrogen ions which are initially in the upstream region. The number of these particles was $N=5000$, and their initial energy was taken to be $\gamma_0=4$; their initial energy distribution was $f(\gamma)=N\delta(\gamma-\gamma_0)$ with an isotropic momentum distribution. Plasma parameters such as $m_{\rm H}/m_e$ and $|\Omega_{e0}|/\omega_{pe}$ were the same as those in the particle simulation.

Figure 8 shows the time variation of γ of an accelerated particle. Here, γ increases stepwise from $\gamma=4$ to $\gamma\simeq120$ by $\Omega_{\rm H0}t=9000$. The acceleration processes have not finished by this time. Figure 9 shows time variations of $X=x-v_{\rm sh}t$, $p_\parallel$, and $p_\perp$. Here, the position of the shock front is taken to be $X=0$; thus, the top panel indicates that the particle barely enters the shock wave. In this and the following figures, X and p are normalized to c/ω_{pe} and $m_{\rm H}c$, respectively. After the encounter with the shock wave, the particle spends most of the time in the upstream region. The middle panel shows that $p_\parallel$ grows steadily. It also shows, however, that $p_\parallel$ slightly decreases when the particle enters the shock wave. This is in accord with the theoretical prediction based on Eq. (32), which this shock wave satisfies. Inspection of the top and bottom panels shows that $p_\perp$ rises when the particle is in the strong-field region and goes down rapidly at the moment when it goes out to the upstream region, which is also in agreement with the theory. Its value in the upstream region, therefore, does not change much. Figure 10 shows the trajec-

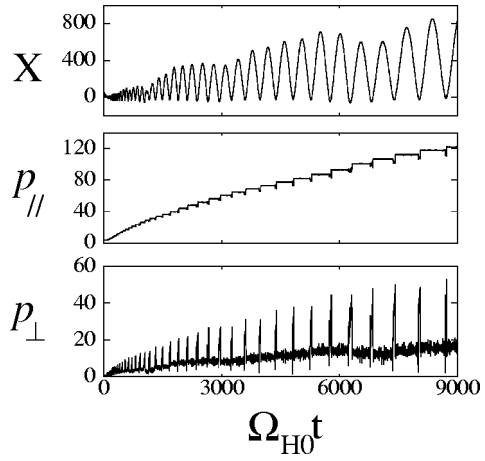

FIG. 9. Time variations of $X=x-v_{sh}t$, $p_\parallel$, and $p_\perp$ of the particle shown in Fig. 8. Here, X is normalized to c/ω_{pe}, and $p_\parallel$ and $p_\perp$ are normalized to $m_H c$. The position of the shock front is taken to be $X=0$.

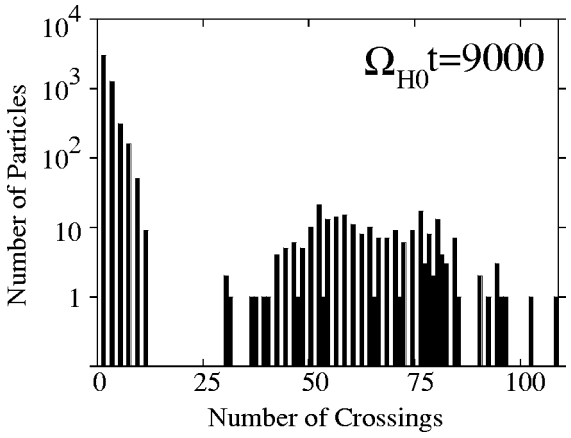

FIG. 11. Number of particles vs crossing times. Of 5000 particles, 239 particles (5%) have crossed the shock front 30 times or more by $\Omega_{H0}t=9000$. The particles with crossing times less than 12 have already moved to the downstream region by this time.

tory of this particle in the $(p_\parallel, p_\perp)$ plane. (The length of the line does not correspond to the length of the time; the changes in $p_\parallel$ and $p_\perp$ are quite small when the particle is in the upstream region where it spends most of the time.) Comparing Figs. 9 and 10, we confirm that, in the phases where $p_\perp$ grows, the particle is in the strong-field region. Also, the rapid decrease in $p_\perp$ takes place at the moments when the particle goes out to the upstream region.

Figure 11 shows how many times these energetic particles crossed the shock front. The present initial velocity distribution corresponds to the middle half circle in Fig. 3. Hence, there were no particles in either region C or D. The number of particles that were initially in regions A and B were 1173 (23%) and 3827 (77%), respectively. The latter is close to the value obtained from Eq. (15); 3800 (76%). Accordingly, all the particles crossed the front at least once. The number of particles that crossed twice or more is 2039 (41%). This indicates that nearly 50% of the particles that were initially in region B have crossed the shock front multiple times. The number of particles that crossed the front less than twelve times is 4761 (95%). These numbers of crossing times are odd; 1, 3, ..., 11. This means that these particles have eventually moved to the downstream region. The other particles (5%) crossed the front 30 times or more. About 92% of them have even numbers of crossing times; they are in the upstream region at $\Omega_{H0}t=9000$.

Figure 12 shows energy distributions of these particles at various times. Each division of γ is $\Delta\gamma=4$. The maximum energy and the number of high-energy particles both gradually increase with time. At $\Omega_{H0}t=9000$, 3.4% of the particles have energies higher than $\gamma=50$, and the maximum energy is $\gamma\simeq 130$. (We stopped calculating the orbits of particles that had moved to the downstream region sufficiently far away from the shock front such that $X<-200c/\omega_{pe}$. For these particles, we use the values of γ and $\boldsymbol{p}$ at the moments the calculation was stopped. This was also the case in Fig. 11.)

Figures 13 and 14 show time evolution of the fast particles in the momentum space; the former displays the early phase, while the latter shows long-time behavior. Regions A, B, and C are also shown. Region D, which is between region C and the horizontal bottom line, is quite narrow in this case. The upper left panel of Fig. 13 shows the initial distribution of the energetic particles. Because their initial energies are

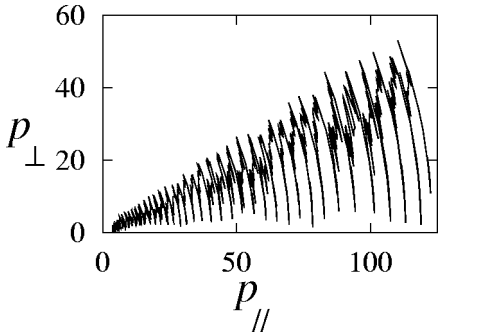

FIG. 10. Trajectory in the $(p_\parallel, p_\perp)$ plane of the particle shown in Figs. 8 and 9. The rapid change in the momentum occurs in each gyroperiod. When the particle is in the upstream region, $p_\parallel$ and $p_\perp$ are almost constant.

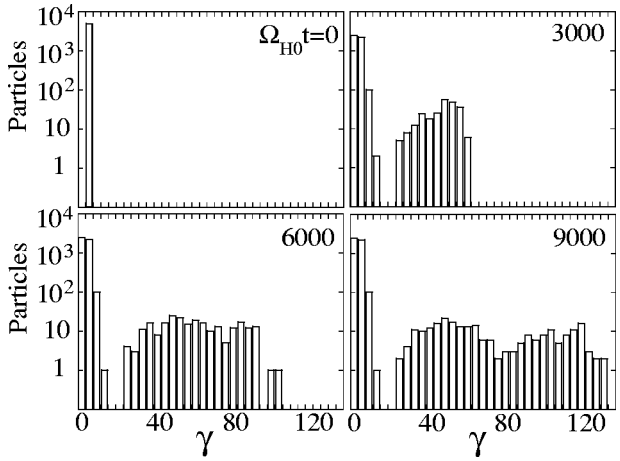

FIG. 12. Evolution of energy distribution. All the particles have the same initial energy, $\gamma=4$, with an isotropic momentum distribution. At $\Omega_{H0}t=9000$, 3.4% of the particles are in the region $\gamma>50$.

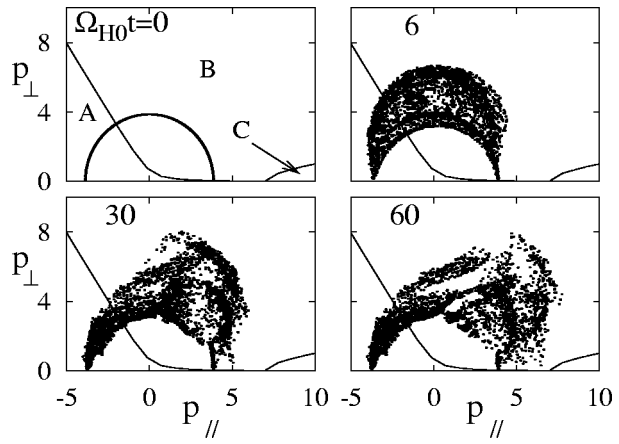

FIG. 13. Evolution of particles in the momentum space $(p_\parallel, p_\perp)$ in the early phase. Initially, the particles are on the half-circle line. Entering the shock wave, $p_{\perp}$'s significantly change (the upper right panel). Then, $p_{\parallel}$'s gradually increase.

the same, $\gamma_0=4$, they are in the half circle in the $(p_\parallel, p_\perp)$ plane; i.e., $p_\perp^2+p_\parallel^2=m_H^2c^2(\gamma_0^2-1)$. As they interact with the shock wave, perpendicular momenta of most of the fast particles increase owing to the transverse electric field (the upper right panel). Parallel momenta of some of them then gradually grow (the lower panels). Figure 14 indicates that the accelerated particles move along the boundary line between regions B and C given by Eq. (8) with $p_{0\parallel}>0$ (namely, $v_{0\parallel}=v_{sh}/\cos\theta_0$ in the velocity space), even though there are no particles around this line initially. The particles with large $p_\perp$ are in the strong-field region at the moment of the snapshot.

IV. SUMMARY

We have discussed the evolution of fast ions incessantly accelerated by oblique shock waves with $v_{sh}\sim c\cos\theta_0$. First, we have analyzed the conditions for particles to cross the shock front multiple times. We then studied the change in the momentum of an energetic particle on crossing the shock front. The perpendicular momentum rises owing to the transverse electric field while the particle is in the strong-field region. The change in $p_\parallel$ is due to the magnetic structure. If the shock propagation speed is high, the parallel momentum decreases at the moment when the particle goes in the shock wave; $p_{1\parallel}(t_{in})<p_{0\parallel}(t_{in})$. It always holds, however, that $p_{0\parallel}(t_{out})>p_{0\parallel}(t_{in})$. Next, with numerical simulations, we studied the evolution of 5000 energetic particles with the initial energy $\gamma=4$ with an isotropic momentum distribution. In this simulation model, field profiles of a shock wave are obtained from a particle simulation. We then calculate long-time trajectories of test energetic particles in these fields. It has been shown that 3.4% of the particles have been accelerated to energies $\gamma>50$ by the time $\Omega_{H0}t=9000$. The development of the particles in the momentum space has also been shown. The momentum distribution spreads along the line (8) ($v_{0\parallel}=v_{sh}/\cos\theta_0$ in the velocity space).

This acceleration mechanism would become important in plasmas in strong magnetic fields (or with low densities) such as those around pulsars.

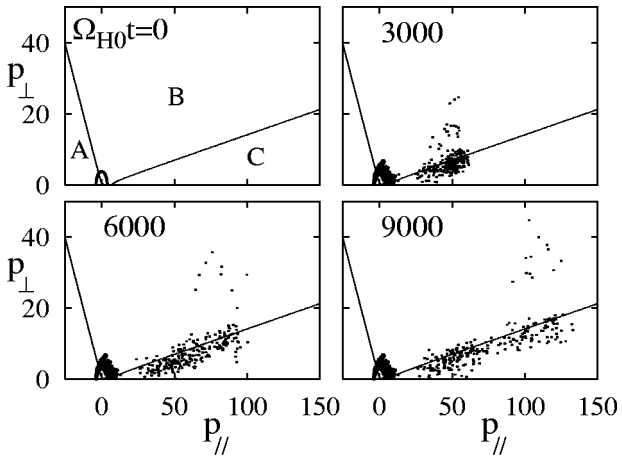

FIG. 14. Long-time evolution of particles in the momentum space $(p_\parallel, p_\perp)$. From the initial half-circle line, accelerated particles spread along the boundary line between regions B and C. The particles with large $p_\perp$, which are found in the panels of $\Omega_{H0}t=3000$, 6000, and 9000, are in the strong-field region at these moments.

ACKNOWLEDGMENTS

This work was carried out by the joint research program of the Solar-Terrestrial Environment Laboratory, Nagoya University, and was supported in part by a Grant-in-Aid for Scientific Research from the Japan Society for the Promotion of Science.

[1] S. Usami, H. Hasegawa, and Y. Ohsawa, Phys. Plasmas **8**, 2666 (2001).
[2] S. Usami and Y. Ohsawa, Phys. Plasmas **9**, 1069 (2002).
[3] T. Masaki, H. Hasegawa, and Y. Ohsawa, Phys. Plasmas **7**, 529 (2000).
[4] D. Biskamp and H. Welter, Nucl. Fusion **12**, 663 (1972).
[5] D. W. Forslund, K. B. Quest, J. U. Brackbill, and K. Lee, J. Geophys. Res., [Oceans] **89**, 2142 (1984).
[6] Y. Ohsawa, Phys. Fluids **28**, 2130 (1985).
[7] B. Lembege and J. M. Dawson, Phys. Fluids B **1**, 1001 (1989).
[8] R. L. Tokar, S. P. Gary, and K. B. Quest, Phys. Fluids **30**, 2569 (1987).
[9] R. Z. Sagdeev and V. D. Shapiro, Zh. Éksp. Teor. Fiz. Pis'ma Red. **17**, 387 (1973) [JETP Lett. **17**, 279 (1973)].
[10] Y. Ohsawa, J. Phys. Soc. Jpn. **59**, 2782 (1990).
[11] M. A. Lee, V. D. Shapiro, and R. Z. Sagdeev, J. Geophys. Res., [Oceans] **101**, 4777 (1996).
[12] M. Toida and Y. Ohsawa, J. Phys. Soc. Jpn. **64**, 2036 (1995).
[13] M. Toida and Y. Ohsawa, Sol. Phys. **171**, 161 (1997).
[14] N. Bessho and Y. Ohsawa, Phys. Plasmas **6**, 3076 (1999).
[15] N. Bessho and Y. Ohsawa, Phys. Plasmas **7**, 4004 (2000).
[16] N. Bessho and Y. Ohsawa, Phys. Plasmas **9**, 979 (2002).
[17] C. S. Gardner and G. K. Morikawa, Commun. Pure Appl. Math. **18**, 35 (1965).
[18] T. Kakutani, H. Ono, T. Taniuti, and C. C. Wei, J. Phys. Soc. Jpn. **24**, 1159 (1968).
[19] Y. Ohsawa, Phys. Fluids **29**, 1844 (1986).
[20] J. H. Adlam and J. E. Allen, Philos. Mag., Suppl. **3**, 448 (1958).
[21] L. Davis, R. Lüst, and A. Schlüter, Z. Naturforsch. A **13**, 916 (1958).
[22] Y. Ohsawa, Phys. Fluids **29**, 2474 (1986).
[23] K. Maruyama, N. Bessho, and Y. Ohsawa, Phys. Plasmas **5**, 3257 (1998).
[24] T. P. Armstrong, G. Chen, E. T. Sarris, and S. M. Krimigis, in *Study of Traveling Interplanetary Phenomena*, edited by M. A. Shea and D. F. Smart (Reidel, Dordrecht, 1977), p. 367.
[25] R. B. Decker, Space Sci. Rev. **48**, 195 (1988).
[26] P. C. Liewer, A. T. Lin, J. M. Dawson, and M. Z. Caponi, Phys. Fluids **24**, 1364 (1981).